FRIGID ZONE **MEDICINE**
Original Article • DOI: 10.1515/fzm-2026-0003

Silencing lipocalin-2 ameliorates severe hypothermia-induced acute lung injury in rats by regulating macrophage polarization

Xin Zheng[1,2#], Yiwei Ding[1#], Fan Wang[1#], Jiajia Tang[1], Zhihai Han[1*], Xuxin Chen[1*]

Abstract

Objective: Severe hypothermia can precipitate acute lung injury (ALI) and may progress to acute respiratory distress syndrome (ARDS). Alveolar macrophage (AM) polarization plays a pivotal role in both the pathogenesis and resolution of ALI/ARDS. This study aimed to investigate alterations in AM polarization and to identify potential regulatory targets of macrophage polarization in severe hypothermia-induced ALI (SH-ALI). **Methods:** An SH-ALI rat model was established by immersion in 15 °C seawater for 5 h. Survival rate, inflammatory cytokine levels, lung histopathology, lung wet-to-dry weight ratio, and AM polarization status were assessed. RNA sequencing was performed to identify differentially expressed genes in bronchoalveolar lavage fluid-stimulated AMs from SH-ALI rats compared with normal AMs. Lipocalin-2 (LCN2) was identified and validated as a differentially expressed gene in SH-ALI. The effects of LCN2 on macrophage polarization, survival rate, lung injury severity, and inflammatory factor levels were further evaluated. **Results:** SH-ALI was characterized by increased mortality, elevated inflammatory cytokine levels, marked inflammatory cell infiltration, aggravated pulmonary edema, and significant pulmonary parenchyma injury. An imbalance between M1 and M2 macrophage polarization was observed, with severe hypothermia promoting M1 polarization. LCN2 expression was significantly upregulated in SH-ALI rats. Downregulation of LCN2 suppressed M1 polarization and alleviated lung injury in SH-ALI in rats. **Conclusion:** Immersion in 15 °C seawater for 5 h successfully establishes an SH-ALI rat model. SH-ALI is associated with excessive M1 polarization, and LCN2 knockdown mitigates lung injury by inhibiting M1 polarization in SH-ALI rats.

Keywords

hypothermia; acute lung injury; lipocalin-2

Received 20 December 2024, accepted 09 January 2026

[1]*Department of Pulmonary and Critical Care Medicine, Sixth Medical Center of PLA General Hospital, Beijing 100048, China*
[2]*Department of Pulmonary and Critical Care Medicine, Taixing People's Hospital, Taixing, 225400, China*

[#]*These authors are co-first authors*
**Corresponding authors Zhihai Han, E-mail: zhihaihandoctor@163.com; Xuxin Chen, E-mail: chenxuxin9478@qq.com*

1 Introduction

Hypothermia is defined as a condition in which the core body temperature falls below 35 °C for various reasons, most commonly due to exposure low-temperature environments, such as prolonged seawater immersion or exposure in high-altitude and cold regions[1]. Based on core body temperature, hypothermia is classified as mild (32.0-35.0 °C), moderate (28.0-31.9 °C), and severe (< 28.0 °C)[2]. Because seawater is typically cold and has high thermal conductivity, heat loss is markedly accelerated when a seafarer falls into the water. As a result, core temperature can decline rapidly, leading to severe hypothermia[3]. Cold seawater immersion has been reported to cause injury to multiple organ systems. Among these complications, acute lung injury (ALI) is one of the most severe occurs at an early stage. Patients with hypothermia-induced lung injury often present with diffuse alveolar edema and hemorrhage, impaired oxygen diffusion, and reduced oxygenation efficiency, which may progress to acute respiratory distress syndrome (ARDS) in severe cases[4].

Previous studies have suggested that the pathogenesis of

severe hypothermia-induced ALI (SH-ALI) pathogenesis may involve several mechanisms, including excessive inflammatory responses, imbalance between oxidation and antioxidative systems, increased immune cell apoptosis, and coagulation disorders[4-7]. Among these factors, uncontrolled inflammation appears to be a central contributor. Alveolar macrophages (AMs) have been reported to play a critical role in the dysregulated inflammatory response observed in ALI/ARDS[8]. Macrophages are generally categorized into two major phenotypes: classically activated or pro-inflammatory (M1) macrophages and alternatively activated or anti-inflammatory (M2) macrophages[9]. Persistent M1 polarization causes excessive and sustained inflammatory responses, thereby promoting the initiation and progression of ALI/ARDS[10]. Accordingly, modulation of macrophage polarization has emerged as a potential therapeutic strategy for ALI/ARDS[11]. However, to date, no studies have systematically characterized macrophage polarization, phenotypic switching, or their functional contribution in SH-ALI.

RNA sequencing (RNA-Seq) technology enables high-throughput and comprehensive profiling of gene expression patterns[12-13]. In the present study, RNA-Seq analysis of the rat alveolar macrophage (AM) cell line NR8383 in an *in vitro* simulated SH-ALI model identified lipocalin-2 (LCN2) as a differentially expressed gene. Previous studies have demonstrated that LCN2 promotes M1 macrophage polarization in a mouse model of cardiac ischemia-reperfusion injury[14]. Whether LCN2 similarly regulates macrophage polarization and contributes to uncontrolled inflammation in SH-ALI remains to be determined.

Therefore, the present study aimed to investigate the alterations and functional significance of macrophage polarization in SH-ALI and to explore the role of LCN2 in regulating macrophage polarization and pulmonary damage in SH-ALI. To this end, an SH-ALI rat model was established by immersing rats in 15 °C seawater for 5 h. The effects of LCN2 on lung injury severity and AM polarization were subsequently evaluated.

2 Methods

2.1 Cell lines and cell culture

The rat AM cell line NR8383 (American Type Culture Collection, Manassas, VA, USA) was cultured in Ham's F12 medium (Gibco; Thermo Fisher Scientific, Inc., Waltham, MA, USA) supplemented with 10% fetal bovine serum (FBS, Gibco). Cells were maintained at 37 °C in a humidified incubator with 5% CO_2. Cells in the exponential growth phase were used all subsequent experiments.

2.2 Lentiviral vector construction and transduction into NR8383 cells

The primers used to construct LCN2 shRNA were 5'-GCATCTGATCCCTCTTATTTG-3' and 5'-CAAATAAGAGGGATCAGATGC-3' (RiboBio Co., Ltd., Guangzhou, China). Short hairpin oligonucleotides targeting the LCN2 consensus sequence and their complementary strands were designed and cloned into the U6-shRNA-EF1-copGFP-2A-PURO expression vector, which carries green fluorescent protein (GFP) and puromycin resistance genes (RiboBio). The recombinant vector, together with pHelper 1.0 and pHelper 2.0 plasmids (RiboBio), was co-transfected into 293T packaging cells to generate the recombinant lentiviral vector Lenti. shLCN2. A lentiviral vector carrying a scrambled shRNA sequence was used as a negative control (Lenti.control; RiboBio). The viral titers of Lenti.shLCN2 and Lenti. control were > 5 × 10^8 TU/mL and 6 × 10^8 TU/mL, respectively. NR8383 cells were seeded and infected with lentivirus at 70%-80% confluence at a multiplicity of infection (MOI) of 25. After 12 h of infection, the medium was replaced with fresh complete medium, and the cells were cultured for an additional 24 h. Puromycin (1 μg/mL) was then added to eliminate uninfected cells, and selection was continued for 24 h. NR8383 cells with reduced LCN2 expression levels in NR8383 cells were thus established. LCN2 expression levels in NR8383 cells were confirmed by quantitative real-time PCR (qRT-PCR).

2.3 Construction of adeno-associated virus (AAV) vector

Based on the interference efficiency observed with the lentiviral vector, the validated target sequence for LCN2 was GCATCTGATCCCTCTTATTTG. The corresponding primer pair for this target sequence was 5'-GCATCTGATCCCTCTTATTTG-3' and 5'-CAAATAAGAGGGATCAGATGC-3' (GeneChem Co., Ltd., Shanghai, China). Short hairpin oligonucleotides targeting LCN2 and their complementary strands were subcloned into the GV407 vector (pAAV-F4/80p-EGFP-MIR155(RNAi)-SV40 PolyA; GeneChem). The recombinant plasmid was d co-transfected with pAAV-RC and pAAV-helper (GeneChem) into 293-AAV cells to generate the recombinant AAV vector designated AAV.shLCN2. An AAV vector carrying a scrambled shRNA sequence was constructed as a negative control (AAV.control; GeneChem). The titers of AAV. shLCN2 and AAV.control were 1 × 10^{13} vg/mL and 2 × 10^{13} vg/mL, respectively.

2.4 Establishment of the SH-ALI rat model and experimental design

Adult Sprague Dawley rats (6-8 weeks old) were purchased from the Laboratory Animal Center of the Academy of Military Medical

Sciences (certificate number: SCXK-Army-2012-0004; Beijing, China). All animal procedures were approved by the Animal Care and Use Committee of the Chinese PLA General Hospital (approval number: SQ2022494) and conducted in accordance with the Animal Research: Reporting of *In vivo* Experiments (ARRIVE) Guidelines on the Use of Laboratory Animals[15]. Experiments were performed in compliance with the National Institutes of Health guidelines for laboratory animal care and Chinese national regulations for experimental animals.

Ten rats were randomly assigned to either the normal (no treatment) or the SH-ALI group (immersed in 15 °C seawater for 5 h), with five rats per group. If animals in the experimental group died during modeling, additional animals were added to maintain the planned sample size. Rectal temperature was monitored every 30 min using a digital thermometer. Five hours after seawater immersion, rats were euthanized with an overdose of pentobarbital sodium (100 mg/kg), and lung tissue, blood, and bronchoalveolar lavage fluid (BALF) samples were collected as previously described[16]. In addition, a second cohort of 30 rats was randomly divided into two groups (15 rats per group) and treated as described above. The 7-h survival rate was recorded and analyzed. After LCN2 was identified as a differentially expressed gene (DEG), its expression in rat lungs was downregulated by intranasal administration of AAV.shLCN2 at a total dose of 4×10^{11} vector genomes in 40 μL per rat using a 1-mL blunt-ended syringe, as previously described[17]. An equal dose of AAV. control was used as a negative control. Lung tissue, blood, and BALF samples were collected, and survival rates were recorded to evaluate the effects of LNC2 knockdown on lung injury severity, inflammation cytokine levels, and AM polarization status.

Cells were treated with 1 mL phosphate-buffered saline (PBS) or BALF collected from SH-ALI rats (sterilized by filtration) for 24 h, after which RNA was extracted for RNA-Seq analysis. In parallel, NR8383 and NR8383-LCN2low cells were treated under the same conditions and harvested for flow cytometry and western blot analyses.

2.5 BALF collection

Bronchoalveolar lavage fluid (BALF) was collected by inserting an 18G sterile catheter (Carelife Co., Ltd., Shanghai, China) into the appropriate bronchopulmonary segment. The right lung was lavaged three times with 4 mL phosphate-buffered saline (PBS) per lavage, and approximately 80% of the instilled volume was recovered. BALF samples were centrifuged at 1000 × g for 10 min at 4 °C to pellet the cells. The supernatant was carefully collected, transferred into sterile Eppendorf tubes, and stored at -80 °C for subsequent experiments. The cell pellets were retained for AM isolation and purification.

2.6 AM isolation and purification

AMs were isolated using a modified published method[18]. After centrifugation, cell pellets were resuspended in RPMI-1640 medium (Gibco) supplemented with 2 mmol/L glutamine, 100 U/mL penicillin, 100 μg/mL streptomycin, and 10% FBS (Gibco) to prepare complete medium. Cells were incubated for 3 h to allow adherence, after which non-adherent cells were removed by washing three times with medium. The remaining adherent cells were considered Ams. Cell purity exceeded 98% as assessed by Giemsa staining and morphological evaluation, and cell viability was greater than 97% as determined by trypan blue exclusion assay. The purified AMs were used for subsequent experiments.

2.7 Histopathological examination

Lung tissues were fixed in 4% paraformaldehyde, dehydrated, embedded in paraffin, sectioned, and stained with hematoxylin and eosin (H&E) for histopathological evaluation. Lung injury was assessed by an observer blinded to the experimental groups according to the following criteria: (1) alveolar hemorrhage and/or congestion; (2) inflammatory cell infiltration; (3) alveolar wall thickening; and (4) alveolar and/or interstitial edema. Each parameter was graded on a five-point scale: 0 = none; 1 = 0 to < 25%; 2 = 25% to < 50%; 3 = 50% to < 75%; and 4 = 75%-100% involvement. The scores for all four parameters were summed to generate a total lung injury score ranging from 0 to 16 points[19]. The scores for hemorrhage, inflammation, edema, and alveolar septal thickening were averaged for each group, and the final score represented the overall severity of lung injury based on these four parameters.

2.8 Lung wet-to-dry weight ratio

The lung wet-to-dry (W/D) weight ratio was determined as an indicator of pulmonary edema. A portion of lung tissue was excised and weighed immediately to obtain the wet weight. The tissue was then dried in an oven at 60 °C for 72 h to obtain the dry weight. The W/D ratio was calculated as the wet weight divided by the dry weight to quantify the degree of pulmonary edema. The weighing scale and drying oven were purchased from AISP Scientific Instrument Co., Ltd. (Wuhan, Hubei, China).

2.9 Cytokine level measurement

Levels of interleukin-6 (IL-6) and tumor necrosis factor α (TNF-α) in BALF and serum samples were measured using commercially available rat ELISA kits (USCNlife, Wuhan, Hubei, China) according to the manufacturer's instructions. Samples were prepared as described above prior to analysis.

2.10 Flow cytometry

Macrophages were digested and resuspended in staining buffer (Beyotime Chemical Co, Jiangsu, China). Cells (1 × 10^6/mL) were incubated with APC-conjugated anti-mouse inducible nitric oxide synthase (iNOS) antibody (1 ： 200, 61-5920-82, Thermo Fisher, USA) and PE-conjugated anti-mouse arginase-1 (Arg-1) antibody (1 ： 200, 12-3697-82, Thermo Fisher, USA) for 30 min at room temperature in the dark. Following incubation, cells were immediately analyzed using flow cytometry. Data were processed using FlowJo software (version 10.0.7r2, FlowJo LLC, Tree Star, USA). Isotype-matched antibodies were used as controls. The positive gate was set to include < 1% events within the distribution peak obtained using the corresponding isotype control antibody.

2.11 RNA-Seq analysis

Total RNA was extracted from NR8383 cells using TRIzol (Invitrogen, Carlsbad, CA, USA) and used to construct cDNA libraries according to the manufacturer's instructions. RNA sequencing was performed on the Illumina NovaSeq 6000 platform. Paired-end clean reads were aligned to the mouse reference genome (Ensemble_GRCm38.90) using HISAT2 (version 2.1.0). Gene expression levels were quantified from the aligned reads using Fastp (version 0.19.7). Differentially expressed genes (DEGs) were identified were analyzed using DESeq2 (version 1.20.0) with statistical significance defined as adjusted *P* value < 0.05 and |log2FoldChange|≥1. Data visualization, including heatmaps and volcano plots, was performed using the ggplot2 package in R. Gene Ontology (GO) and Kyoto Encyclopedia of Genes and Genomes (KEGG) enrichment analyses were performed using the ClusterProfiler R package (version 3.8.1) to explore the biologica functions and pathways associated with the DEGs. Key DEGs were further validated in AMs isolated from BALF by RT-PCR.

2.12 RT-PCR

Total RNA samples were isolated from cultured cells or lung tissues using Trizol (Invitrogen, Carlsbad, CA, USA) and further purified with an RNA Cleanup Kit (CWBIO Co., Beijing, China). Reverse transcription was performed using a Takara reagent kit (Takara Biotechnology, Otsu, Japan) according to the manufacturer's instructions. Quantitative real-time PCR was carried out using FastStart Universal SYBR Green Master Mix (Yeasen Biotechnology Co., Ltd., Shanghai, China) to determine relative mRNA expression levels. Rat GAPDH was used as the internal reference gene. All reactions were performed in triplicate. Data were analyzed using Rotor-Gene Real-Time Analysis Software 6.0 (Corbett Research, Sydney, Australia). Relative gene expression levels were calculated using the 2−ΔΔCt method. The primer sequences used for quantitative PCR are listed in Table 1.

Table 1 Primer sequences used for quantitative PCR

Target	Forward Primer (5'-3')	Reverse Primer (5'-3')
Ldlr	CATTTTCAGTGCCAACCGCC	TGCCTCACACCAGTTTACCC
Dhcr24	GCCCTTGGTGTCTATGGGTC	CAGGATTAGCTCGTAGGCCG
Cyp51	CCAGCCGAGGACATTCTTCA	CCGCACACCGTTTTCTGTTC
LCN2	GCTGTCGCTACTGGATCAGA	TCGCTCCTTCAGTTCATCGG
CCr7	TGTGTGACTTCAACTGCCCA	GCACATCCTTCTTGAAGCAC
Ccl2	CACTCACCTGCTGCTACTCA	CCTTATTGGGGTCAGCACAGA
Fabp4	ATGGTGGGGTCCTGGTACAT	CTTGGCTCATGCCCTTTCGT
Clec7a	CATCCCAAACTACAGGCGTC	ACTTGAAACGAGTTGGGGGT
Acsl1	TGTGGGGTGGAAATCATCGG	CATTGCTCCTTTGGGGTTGC
Cybb	TGCCAGTGTGTCGGAATCTC	TGTGAATGGCCGTGTGAAGT
Agt	GCACGACTTCCTGACTTGG	ACTCTGTGGGCTGCTCCTCC
GAPDH	CGTGTTCCTACCCCCAATGT	AGGAGACAACCTGGTCCTCA

2.13 Western blot

Total protein was extracted from treated cells using standard procedures. Western blot analysis was performed as previously described[20]. Equal amounts of protein were separated by 15% sodium dodecyl sulfate–polyacrylamide gel electrophoresis and transferred onto polyvinylidene difluoride membranes (Beyotime). Membranes were blocked with 5% (w/v) nonfat milk and incubated overnight at 4 °C with the following primary antibodies: rabbit anti-iNOS (1 ： 1000, ab15323, Abcam, Cambridge, UK), rabbit anti-rat-Arg-1 (1 ： 1000, 93668S, Cell Signaling Technology, Boston, USA), and rabbit anti-rat-LCN2 (1 ： 1000, ab216462, abcam, Cambridge, UK). After washing, membranes were incubated with species-matched horseradish peroxidase-conjugated IgG secondary antibodies (Beijing Zhongshan Golden Bridge Biotechnology Co., Ltd., Beijing, China). Protein bands were visualized using enhanced chemiluminescence following the manufacturer's instructions (Beyotime). Band intensities were quantified using Quantity One software (version 4.62, Bio-Rad Laboratories, Inc., Hercules, CA, USA) and normalized to GAPDH (1 ： 1000, NB300-320, Novus Biologicals, LLC, Littleton, CO, USA).

2.14 Immunofluorescence analyses

Immunofluorescence staining was performed on freshly frozen, acetone-fixed 5-μm sections of optimal cutting temperature (OCT)-embedded lung tissue samples. Sections were permeabilized with 0.2% Triton X-100 in PBS for 15 min and blocked with 5% bovine serum albumin for 45 min at room temperature. Slides were then incubated overnight at 4 °C with rabbit polyclonal anti-F4/80 (1 ： 200, ab6640, Abcam, Cambridge, UK), rabbit polyclonal anti-iNOS (1 ： 200, ab15323, Abcam, Cambridge,

UK), or rabbit polyclonal anti-Arg-1 (1 ： 200, 93668S, Cell Signaling Technology, Boston, USA) antibodies. After three washes with PBS, sections were incubated with the appropriate fluorophore-conjugated secondary antibody for 60 min at room temperature in a humidified chamber. The slides were then washed once, counterstained with DAPI (Southern Biotech, England), and washed again after 10 min. Sections were mounted and air-dried. Fluorescence images were captured using a fluorescence microscope (Olympus, Tokyo, Japan) and analyzed using Image J software (National Institutes of Health, Bethesda, MD, USA). Cell counts were performed on images captured at 40 × magnification by two independent investigators and averaged. At least 5 animals per group and two sections per animal were analyzed.

2.15 Statistical analysis

Data are presented as the means ± standard deviation (SD) from the indicated number of independent experiments or biological replicates. Statistical analyses were performed using SPSS 20.0 software (SPSS Inc., Chicago, IL, USA). For post hoc analysis, the Student–Newman–Keuls test was used when variances were homogeneous and the design was balanced, whereas Dunnett's T3 test was applied when variances were unequal. Comparisons between two groups were performed using the two-tailed Student's *t*-test. Survival data were analyzed using Kaplan-Meier curves and the log-rank test. Homogeneity of variance was assessed by Levene's test. A P value < 0.05 was considered statistically significant.

3 Results

3.1 Severe hypothermia induces ALI and promotes M1 macrophage polarization in rats

The initial rat rectal temperature of rats prior to immersion was 32 ± 0.5 °C in both groups. In the SH-ALI group, rectal temperature decreased to 18 ± 0.5 °C within 30 min after seawater immersion and further declined to 15 ± 0.5 °C after 2 h, where it stabilized. In contrast, no significant changes in anal temperature were observed in the normal group (P < 0.05 *vs.* SH-ALI group; Fig. 1a). After 5 h of seawater immersion, rats in the SH-ALI group exhibited limb movement disorders, reduced respiratory rate and amplitude, and loss of consciousness. The survival rate in the SH-ALI group was significantly lower than that in the normal group. Over a 7-h observation period, the survival rate in the SH-ALI group was 30% (P < 0.05 *vs.* normal group; Fig. 1b). Elevated serum inflammatory cytokines reflect systemic inflammation associated with ALI. Thus, serum levels of the IL-6 and TNF-α were measured. Both IL-6 and TNF-αlevels were significantly increased in the SH-ALI group compared with the normal group (P < 0.05 *vs.* normal group, Fig. 1c-1d).

Histopathological examination showed that lung sections from the normal group displayed intact alveolar architecture, without evidence of alveolar space expansion or collapse, neutrophil infiltration, congestion, or hemorrhage. In contrast, lung sections from the SH-ALI group exhibited typical pathological features of ALI, including alveolar collapse, marked thickening of alveolar walls, alveolar congestion and hemorrhage, and substantial neutrophil infiltration (Fig. 1e). To further assess pulmonary vascular permeability and tissue injury, lung W/D ratios and lung injury scores were evaluated. Both the W/D ratio and lung injury score were significantly increased in the SH-ALI group compared with the normal group (P < 0.05; Fig. 1f-1g).

Flow cytometry was performed to assess the expression of iNOS (M1 marker) and Arg-1 (M2 marker) in AMs isolated from BALF after seawater immersion. The results demonstrated that M1/M2 ratio was significantly increased in the SH-ALI group compared to the normal group (P < 0.05; Fig. 1h-1l). Consistently, RT-qPCR analysis showed increased iNOS mRNA expression and decreased Arg-1 mRNA expression in the SH-ALI group (P < 0.05 *vs.* normal group; Fig. 1j-1k)

3.2 Identification and GO/KEGG enrichment analysis of DEGs in BALF-stimulated NR8383 cells compared with normal NR8383 cells

To identify key genes involved in the pathogenesis of SH-ALI, comparative transcriptome analysis was performed using RNA-Seq in NR8383 cells stimulated with BALF from SH-ALI rats and in untreated NR8383 cells. RNA-Seq analysis revealed a substantial number of DEGs in BALF-stimulated NR8383 cells compared to normal NR8383 cells (Fig. 2a-2b). GO enrichment analysis revealed that these DEGs were associated with a variety of biological processes, including interferon-γ production, inflammatory response, reactive oxygen species generation and metabolism, sterol and lipid metabolic processes, and small-molecule biosynthesis (Fig. 2c-2d). KEGG pathway analysis further demonstrated that DEGs were significantly enriched in multiple pathways, such as the adipocytokine signaling pathway, viral protein interaction with cytokine and cytokine receptor, NOD-like receptor signaling pathway, and ferroptosis (Fig. 2e). Among the identified DEGs, lipocalin-2 (LCN2) was markedly upregulated in BALF-stimulated NR8383 cells compared to normal NR8383 cells. RT-qPCR validation confirmed that LCN2 expression was significantly increased in AMs isolated from the BALF of SH-ALI rats compared to those from normal rats (Fig. 2f; P < 0.05).

3.3 LCN2 knockdown suppresses M1 polarization in NR8383 cells

Rats and NR8383 cells were treated as described in the

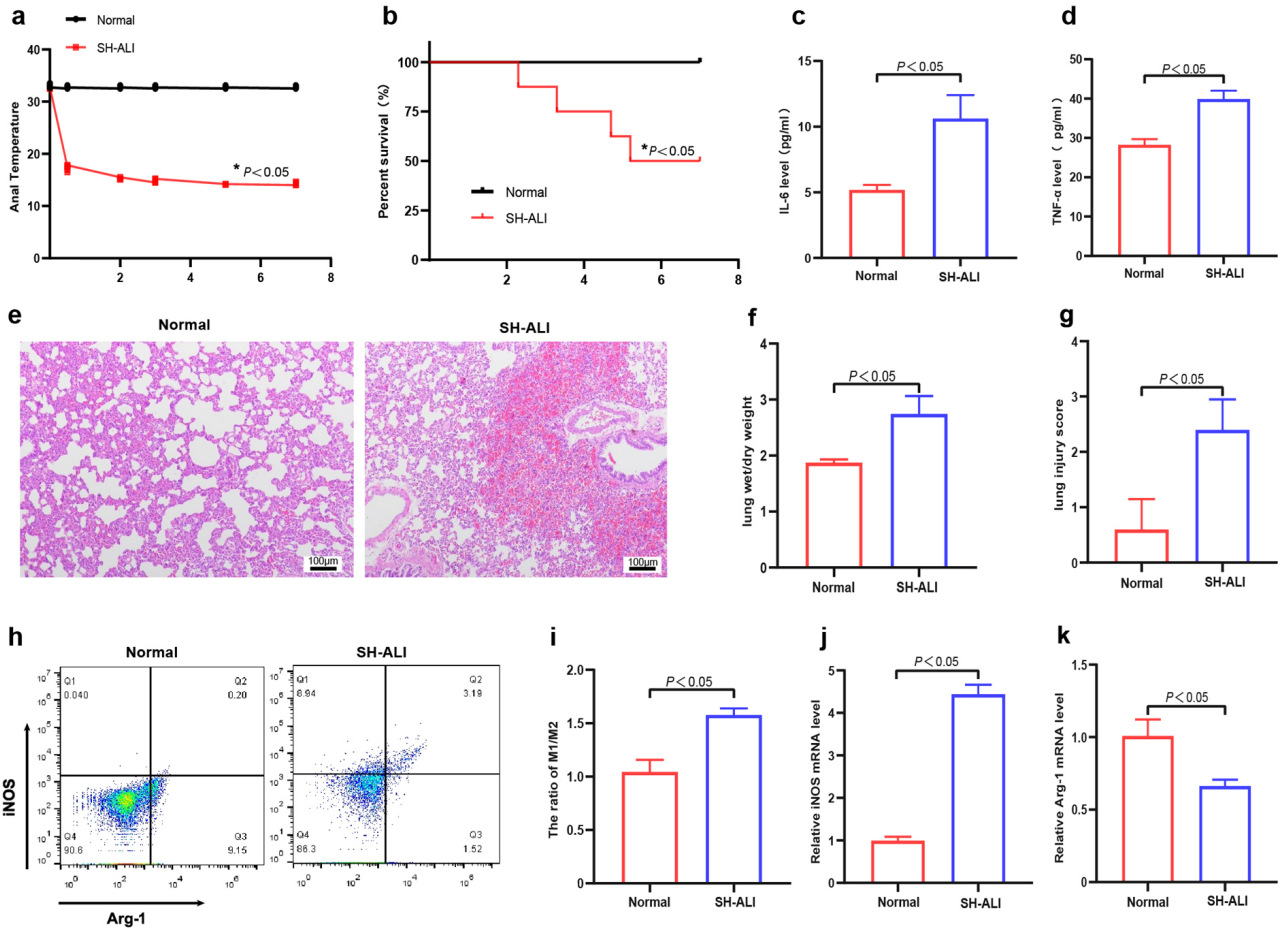

Fig. 1 Establishment of the SH-ALI rat model and AM polarization in SH-ALI rats

(a) Rectal temperature of rats in normal and SH-ALI groups. Data are expressed as means ± SD (n = 5). $^{*}P < 0.05$ *vs.* normal group. (b) Survival rate of rats in the normal and SH-ALI groups. Survival was monitored for 7 h, and survival curves were compared using the log-rank test. Data are expressed as survival percentage (n = 15). $^{*}P < 0.05$ *vs.* normal group. (c-d) Serum levels of inflammatory cytokines IL-6 (c) and TNF-α (d). (e) Representative hematoxylin and eosin (H&E)-stained lung tissue sections. (f) Lung wet-to-dry (W/D) weight ratios in the normal and SH-ALI groups. (g) Lung injury scores in the normal and SH-ALI groups. (h-k) Severe hypothermia promotes M1 polarization: (h) Representative flow cytometry plots showing iNOS and Arg-1 expression in AMs isolated from BALF in each group. (i) Quantitative analysis of the $iNOS^{+}$/$Arg\text{-}1^{+}$ ratio in each group. (j-k) mRNA expression levels of the M1 marker iNOS (j) and M2 marker Arg1 (k) in AMs isolated from BALF, as determined by qRT-PCR. Data are expressed as means ± SD (n = 5). $^{*}P < 0.05$ *vs.* normal group. Abbreviations: SH-ALI, severe hypothermia-induced acute lung injury; AM, alveolar macrophage; IL-6, interleukin-6; TNF-α, tumor necrosis factor-α; H&E, hematoxylin and eosin; BALF, bronchoalveolar lavage fluid; iNOS, inducible nitric oxide synthase; Arg-1, arginase-1.

Methods section, and samples were collected at the indicated time points (Fig. 3a). The polarization status of NR8383 cells in each group was assessed 24 h after stimulation with BALF from SH-ALI rats. Western blot analysis showed that the expression of M1 marker iNOS was significantly increased following stimulation with SH-ALI BALF (Fig. 3b-3c). Notably, downregulation of LCN2 markedly attenuated the BALF-induced upregulation of iNOS expression ($P < 0.05$ *vs.* NR8383 + BALF and NR8383 + Lenti.control + BALF groups). In contrast, the expression of the M2 marker Arg-1 was significantly decreased after SH-ALI BALF stimulation. LCN2 knockdown reversed this effect and significantly increased Arg-1 expression in cells treated with SH-ALI BALF (Fig. 3d-3e; $P < 0.05$ *vs.* NR8383 + BALF and NR8383 + Lenti.control + BALF groups). Consistent with these findings, flow cytometry analysis demonstrated that the M1/M2 ratio was significantly decreased in LCN2-knockdown cells following SH-ALI BALF stimulation compared with control groups (Fig. 3f-3g; $P < 0.05$ *vs.* NR8383 + BALF and NR8383 + Lenti.control + BALF groups). These results indicate that LCN2 knockdown suppresses BALF-induced M1 polarization in NR8383 cells.

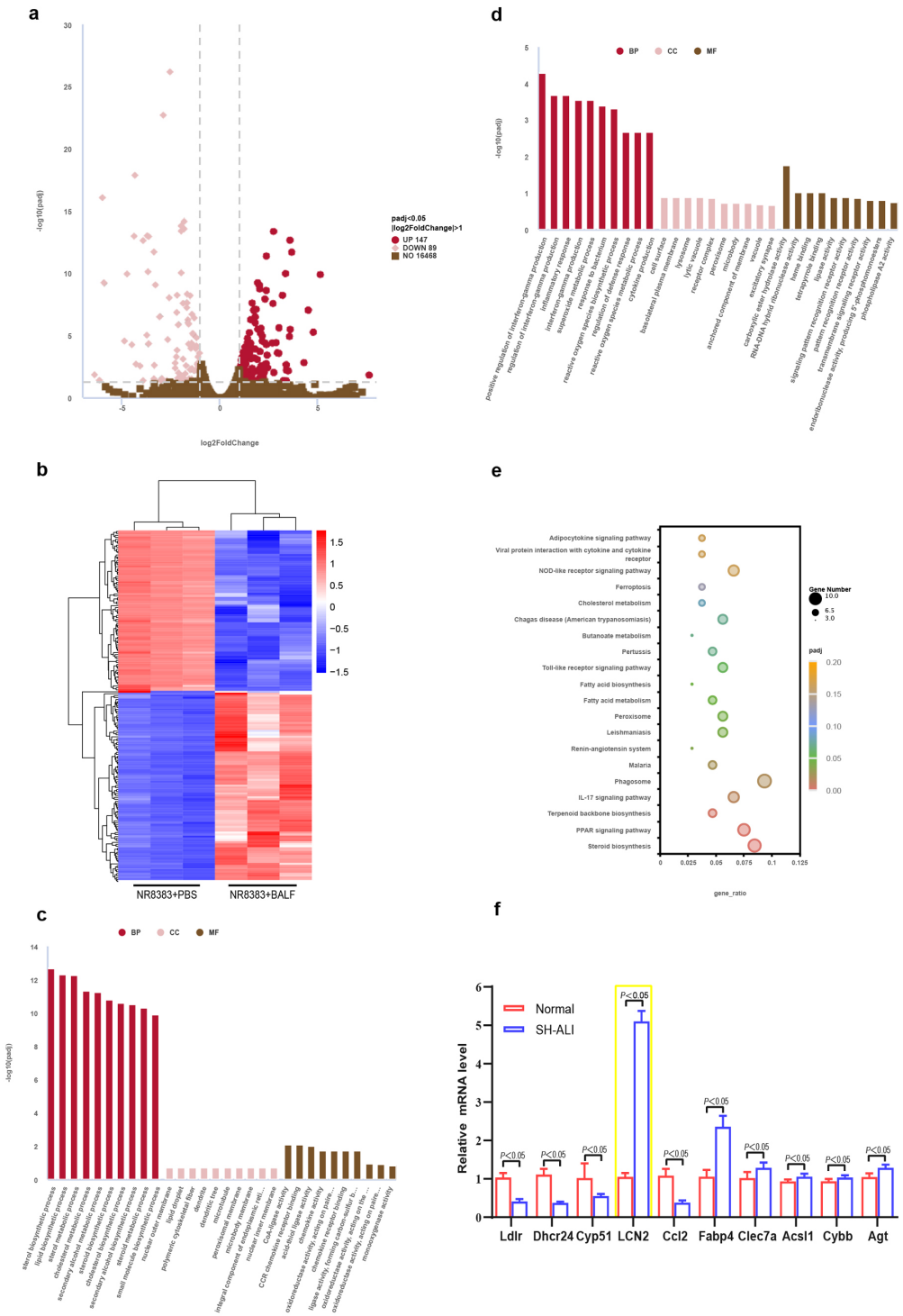

Fig. 2 RNA-Seq analysis of NR8383 cells stimulated with BALF from SH-ALI rat

(a) Volcano plot of DEGs between the NR8383+PBS and NR8383+BALF groups. (b) Hierarchical clustering heatmap of DEGs. (c-d) GO enrichment analysis of upregulated (c) and downregulated (d) genes. (e) KEGG pathway enrichment analysis of DEGs. (f) mRNA expression levels of selected differentially expressed genes in AMs isolated from BALF in each group, as determined by qRT-PCR. Data are expressed as means ± SD (n = 3). Abbreviations: PBS, phosphate-buffered saline; BALF, bronchoalveolar lavage fluid; GO, Gene Ontology; KEGG, Kyoto Encyclopedia of Genes and Genomes; AM, alveolar macrophage.

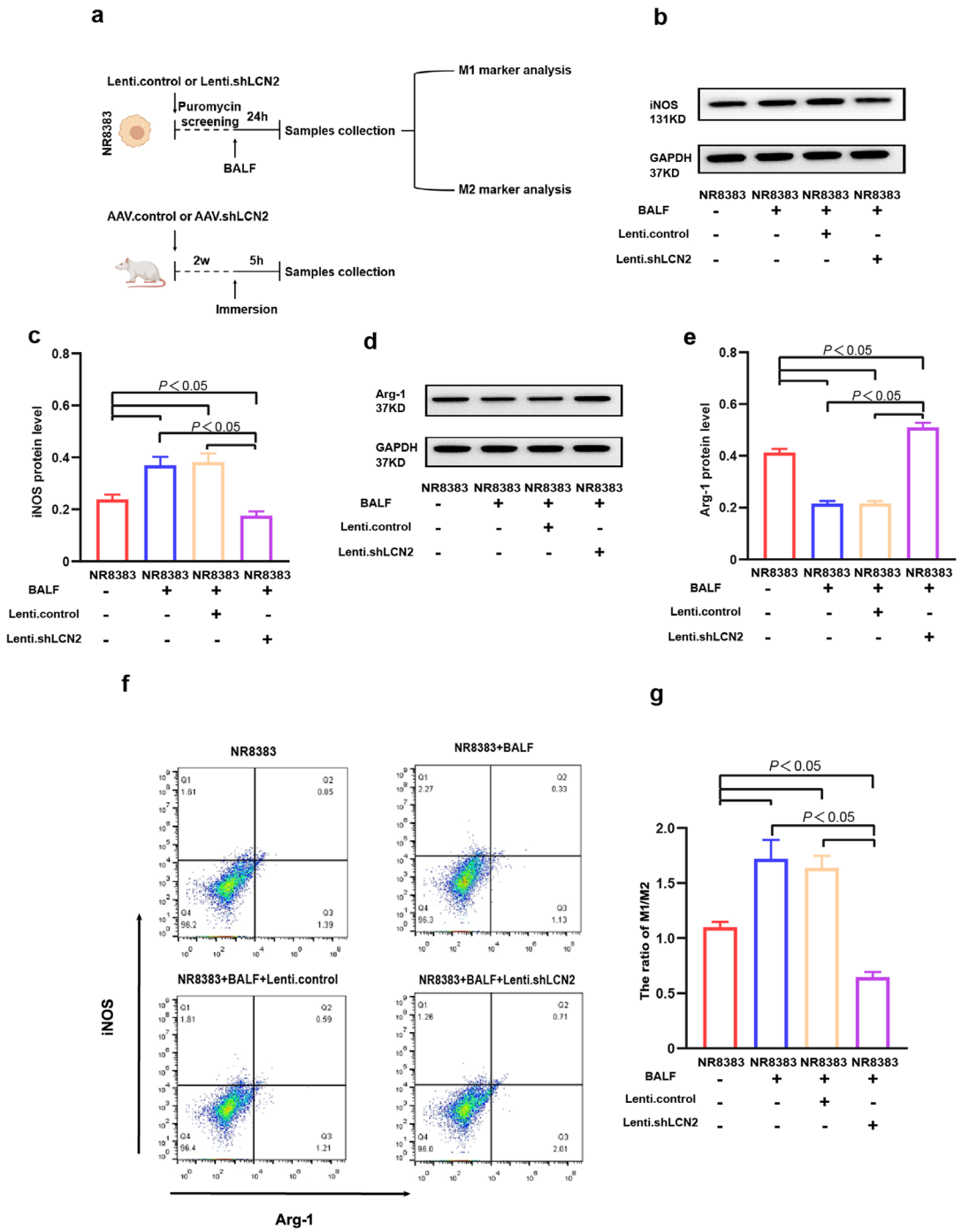

Fig. 3 LCN2 knockdown suppresses M1 polarization in NR8383 cells

(a) Schematic diagram of the experimental design showing the time points of viral transfection, seawater immersion, and sample collection. (b) Representative western blot images showing iNOS protein expression (normalized to GAPDH) in each group. (c) Quantitative analysis of iNOS protein expression normalized to GAPDH. (d) Representative western blot images showing Arg-1 protein expression (normalized to GAPDH) in each group. (e) Quantitative analysis of Arg-1 protein expression normalized to GAPDH. (f) Representative flow cytometry plots showing iNOS and Arg-1 expression in each group. (g) Quantitative analysis of the $iNOS^{+}$/$Arg\text{-}1^{+}$ ratio in each group. Data are expressed as means ± SD ($n = 3$). Abbreviations: LCN2, lipocalin-2; iNOS, inducible nitric oxide synthase; GAPDH, glyceraldehyde-3-phosphate dehydrogenase; Arg-1, arginase-1.

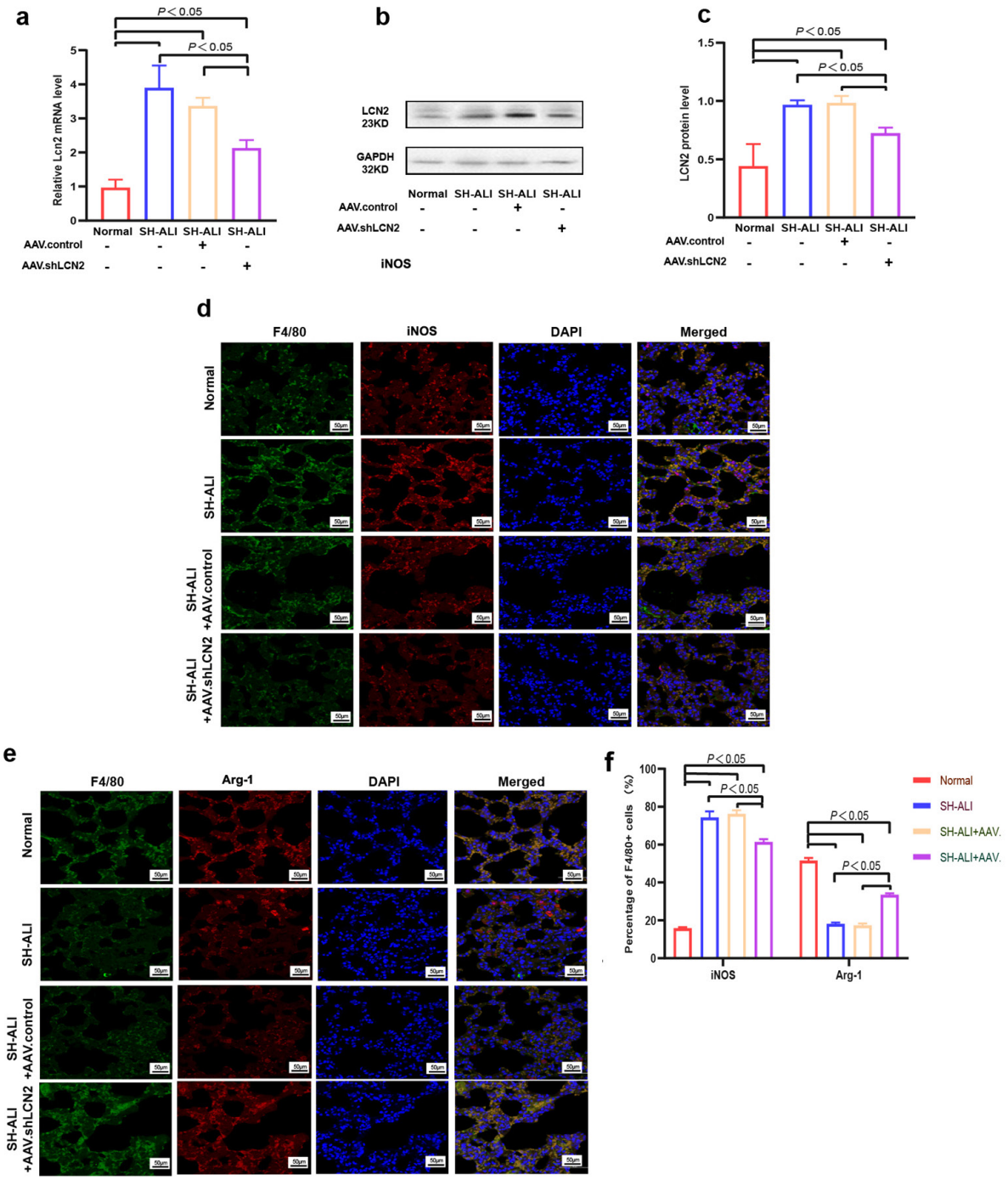

Fig. 4 LCN2 knockdown suppresses M1 polarization in SH-ALI rats

(a) RelativLCN2 mRNA levels normalized to GAPDH in rat Ams, as determined by qRT-PCR. (b) Representative western blot images showing LCN2 protein expression normalized to GAPDH in rat AMs. (c) Quantitative analysis of LCN2 protein expression normalized to GAPDH in rat AMs. (d) Immunofluorescence staining of rat lung tissues showing F4/80 (green), iNOS (red), and DAPI (blue; nuclear counterstain). (e) Immunofluorescence staining of rat lung tissues showing F4/80 (green), Arg-1 (red), and DAPI (blue; used as counterstain for nuclei) in each group. (f) Quantitative analysis of the proportion of $iNOS^+$ or $Arg\text{-}1^+$ cells among F4/80-positive cells in rat lung tissues. Data are presented d as means ± SD (n = 5). Abbreviations: LCN2, lipocalin-2; iNOS, inducible nitric oxide synthase; GAPDH, glyceraldehyde-3-phosphate dehydrogenase; Arg-1, arginase-1.

3.4 LCN2 knockdown suppresses M1 polarization in SH-ALI rats

Rats were pretreated with AAV.control or AAV.shLCN2 *via* intranasal administration prior to seawater immersion. Two weeks later, the SH-ALI model was established by immersing the rats in 15 °C seawater for 5 h. AMs were subsequently isolated from BALF for further analysis. Both mRNA and protein levels of LCN2 in AMs were significantly increased in the SH-ALI and SH-ALI + AAV.control groups, indicating that severe hypothermia markedly upregulated LCN2 expression (Fig. 4a-4c). In contrast, administration of AAV.shLCN2 significantly attenuated the hypothermia-induced increase in LCN2 expression ($P < 0.05$ *vs.* SH-ALI and SH-ALI + AAV.control groups). Double immunofluorescence staining was performed to evaluate macrophage polarization. $iNOS^+F4/80^+$ double-positive cells were identified as M1 macrophages, whereas $Arg\text{-}1^+F4/80^+$ double-positive cells were considered M2 macrophages. The number of $iNOS^+F4/80^+$ cells was markedly increased in the SH-ALI and SH-ALI + AAV.control groups (Fig. 4d-4f). However, compared to with these groups, the number of $iNOS^+F4/80^+$ cells was significantly decreased in the SH-ALI + AAV.shLCN2 group, with a significant increase in the SH-ALI + AAV.shLCN2 group compared with the SH-ALI and SH-ALI + AAV.control groups ($P < 0.05$). Conversely, the number of $Arg\text{-}1^+F4/80^+$ cells exhibited the opposite pattern ($P < 0.05$). These findings indicate that LCN2 knockdown suppresses M1 polarization and promotes M2 polarization in SH-ALI rats.

3.5 LCN2 knockdown attenuates SH-ALI

The 7-h survival rates were 40% in the SH-ALI group and 60% in the SH-ALI + AAV.control group (Fig. 5a). In contrast, rats pretreated with AAV.shLCN2 exhibited a significantly higher survival rates (80%) compared with both the SH-ALI and SH-ALI + AAV.control groups (Fig. 5a; $P < 0.05$). No significant difference in survival was observed between the SH-ALI and SH-ALI + AAV.control groups ($P > 0.05$; Fig. 5a). Histopathological examination of lung tissues revealed that, following seawater immersion, the SH-ALI and SH-ALI + AAV.control groups displayed typical features of severe lung injury, including diffuse alveolar damage, extensive neutrophil infiltration, alveolar congestion and hemorrhage, and pronounced interstitial edema. In contrast, lung injury severity and the corresponding lung injury scores were significantly reduced in the SH-ALI + AAV.shLCN2 group compared with e in the SH-ALI and SH-ALI + AAV.control groups ($P < 0.05$; Fig. 5b-5c). Assessment of pulmonary edema by lung W/D weight ratio showed a marked increase in all seawater-immersed groups compared with the normal group ($P < 0.05$). However, the W/D ratio in the SH-ALI + AAV.shLCN2 group was significantly lower than that in the SH-ALI and SH-ALI + AAV control groups ($P < 0.05$; Fig. 5d). Inflammatory cytokine levels in BALF and serum were further measured by ELISA. TNF-α and IL-6 levels were minimal in the normal group (Fig. 5e-5f). Severe hypothermia markedly increased TNF-α and IL-6 concentrations in both BALF and serum. Importantly, LCN2 knockdown *via* AAV.shLCN2 significantly attenuated the hypothermia-induced elevation of TNF-α and IL-6 levels in BALF and serum ($P < 0.05$ *vs.* SH-ALI and SH-ALI + AAV.control groups). These findings indicate that LCN2 downregulation alleviates lung injury and systemic inflammation in SH-ALI rats.

4 Discussion

The present study yielded several important findings. First, severe hypothermia induced by immersion in 15 °C seawater for 5 h in ALI, characterized by increased mortality, elevated inflammation cytokine levels, inflammatory cell infiltration, aggravated pulmonary edema, and marked pulmonary parenchymal damage. Second, a clear imbalance between M1 and M2 macrophage polarization was observed in SH-ALI, with severe hypothermia promoting polarization toward the pro-inflammatory M1 phenotype. Third, LCN2 expression was significantly upregulated in SH-ALI rats, and LCN2 downregulation suppressed M1 polarization and ameliorated lung injury. To our knowledge, this is the first study demonstrating that LCN2 aggravates pulmonary inflammation and tissue damage by promoting macrophage polarization toward the M1 phenotype in SH-ALI. These findings suggest that targeting LCN2 in macrophages, or in specific macrophage subsets, may represent a potential therapeutic strategy for SH-ALI.

Seawater immersion–induced hypothermia most commonly occurs in individuals who fall overboard at sea, and the lung is one of the most primary target organs[21]. Accidental hypothermia can lead to respiratory depression, impaired oxygenation, asphyxia, and even progression to ALI/ARDS[22-23]. Previous seawater immersion models have mainly been established in anesthetized rabbits, dogs, and other large animals, with research focusing primarily on arrhythmia mechanisms, often overlooking pulmonary injury. However, severe hypothermia complicated by lung injury is a major cause of mortality among individuals exposed to cold seawater[4]. Therefore, detailed investigation of SH-ALI is warranted.

A reliable animal model is essential for exploring disease mechanisms. To date, there have been no describing a rat model of SH-ALI. In the present study, immersion in 15 °C seawater for 5 h successfully induced lung injury in rats, as evidenced by typical histopathological features of ALI, increased lung vascular permeability, and elevated serum inflammatory cytokines. These features are consistent with the key charac-

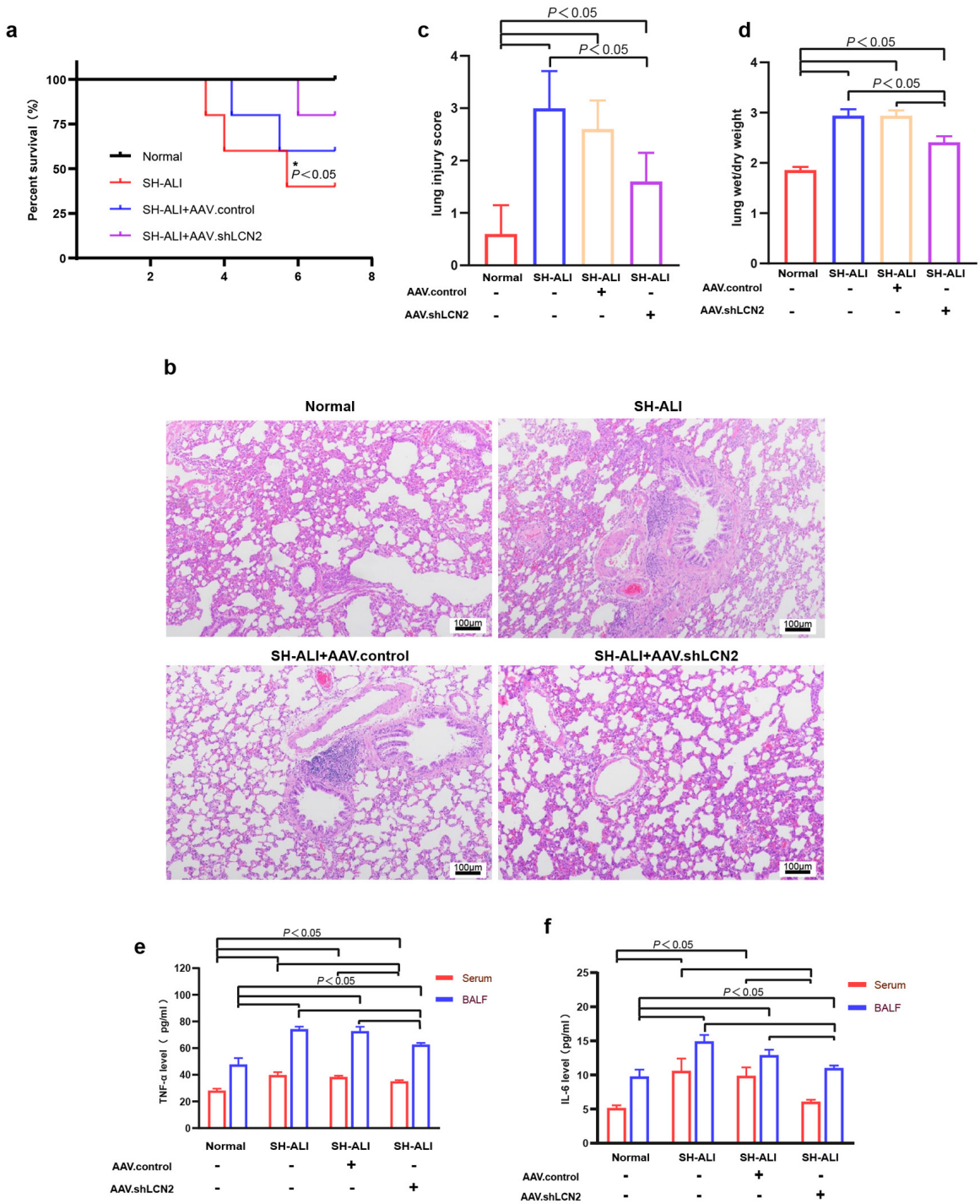

Fig. 5 LCN2 knockdown attenuates SH-ALI

(a) Survival rate of rats in each group. Survival was monitored for 7 h, and survival curves were compared using log-rank test. Data are expressed as survival percentage. $^{*}P < 0.05$ *vs.* SH-ALI + AAV.shLCN2 group. (b) Representative hematoxylin and eosin (H&E)-stained lung tissue sections from each group. (c) Lung injury scores in each group. (d) Lung wet-to-dry (W/D) weight ratios in each group; (e-f) Levels of inflammatory cytokines TNF-α (e) and IL-6 (f) in serum and BALF from each group. Data are expressed as means ± SD ($n = 5$). Abbreviations: LCN2, lipocalin-2; SH-ALI, severe hypothermia-induced acute lung injury; IL-6, interleukin-6; TNF-α, tumor necrosis factor-α; BALF, bronchoalveolar lavage fluid.

teristics of experimental ALI described in the American Thoracic Society Workshop report[24]. Moreover, the 7-h survival rate of 30%-40% indicates that the model is severe yet controllable. Previous data from our group showed that 12 h of immersion at 15 °C resulted in 100% mortality[5], further supporting that 5 h of immersion represents an appropriate and reproducible duration for modeling SH-ALI.

AMs are the most abundant immune cells in the alveolar space and play central roles in all stages of ALI/ARDS[25]. The importance of macrophage polarization in lipopolysaccharide (LPS)- and sepsis-induced ALI has been extensively described[8-9]. However, whether macrophage polarization contributes to SH-ALI had not been investigated. The present study demonstrates that severe hypothermia promotes AM polarization toward the M1 phenotype, accompanied by increased expression of M1-associated genes (TNF-α and IL-6) and the M1 marker iNOS, along with reduced expression of the M2 marker Arg-1. These findings indicate that excessive M1 polarization contributes to inflammatory amplification and lung injury in SH-ALI. With the rapid development of single-cell transcriptomics, additional macrophage subsets beyond the classical M1/M2 paradigm have been identified[26]. Whether unique macrophage subsets emerge during hypothermia-induced lung injury requires further investigation.

Because excessively low culture temperatures impair *in vitro* cell viability, direct cold exposure models are limited for mechanistic studies. In the present study, BALF derived from SH-ALI rats was used to stimulate NR8383 cells, thereby mimicking the inflammatory microenvironment of hypothermia-induced lung injury. This strategy has been adopted in previous studies[27-28] and reflects the cytokine- and metabolite-rich milieu surrounding AMs *in vivo*. RNA-Seq analysis identified several differentially expressed genes, among which LCN2 was significantly upregulated. GO and KEGG enrichment analyses highlighted inflammatory and metabolic pathways, and qRT-PCR validation confirmed increased LCN2 expression e during SH-ALI.

LCN2 is an acute time-phase response protein widely expressed in macrophages, epithelial cells, neutrophils, and eosinophils[29]. Its role in macrophage polarization appears context-dependent. In cardiac ischemia-reperfusion injury, LCN2 promotes M1 polarization[14], and in experimental autoimmune encephalomyelitis, it shapes a pro-inflammatory macrophage phenotype[30]. In ARDS models, LCN2 is upregulated and promotes lung injury, partly through iron accumulation and pro-inflammatory macrophage differentiation[31-32]. In the neonatal LPS induced ARDS mouse model, LCN2 silencing suppressed inflammation and oxidative stress *via* inhibition of MAPK/ERK pathway[33]. Conversely, in gut-origin sepsis, LCN2 may exert protective effects by preserving microbiota homeostasis and limiting oxidative stress[34]. Additional studies have reported divergent roles depending on disease context[35-37]. Therefore, LCN2 cannot be categorized as exclusively pro-inflammatory or protective; its effects depend on the triggering stimulus, cell type, disease phase, and model[38].

In the present study, LCN2 knockdown significantly inhibited M1 polarization and reduced lung injury severity, inflammatory

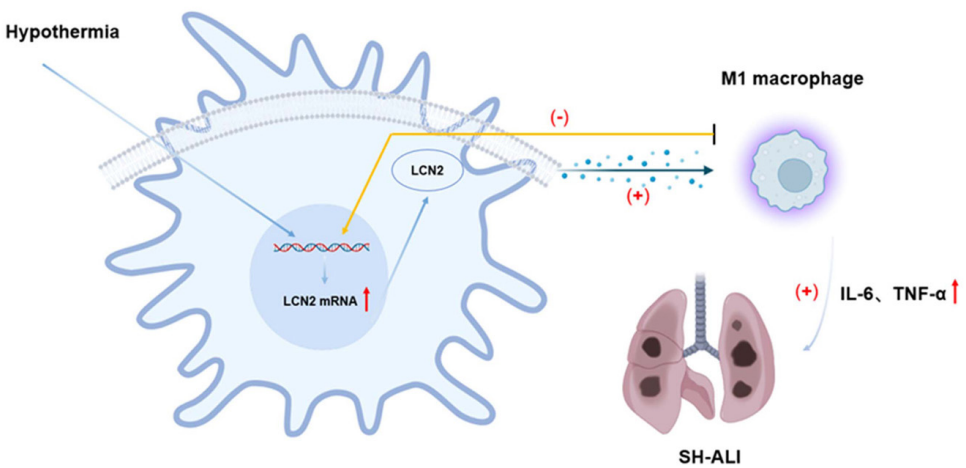

Fig. 6 Schematic illustration of the promotive role of LCN2 in M1 polarization and SH-ALI

Hypothermic stimulation upregulates LCN2 expression in the lung. Elevated LCN2 promotes macrophage polarization toward the M1 phenotype, leading to increased release of pro-inflammatory mediators and amplification of the inflammatory response. This process ultimately contributes to the development of ALI and may progress to ARDS. Silencing of LCN2 attenuates lung injury by inhibiting M1 polarization and reducing inflammatory cytokine production in SH-ALI rats. Abbreviations: LCN2, lipocalin-2; ALI, acute lung injury; SH-ALI, severe hypothermia-induced acute lung injury; ARDS, acute respiratory distress syndrome. Symbols: (-) indicates inhibition; (+) indicates promotion.

cytokine levels, and mortality in SH-ALI rats. Given the established link between classically activated M1 and uncontrolled inflammatory damage in ALI[8], these findings suggest that LCN2 exacerbates SH-ALI by promoting pro-inflammatory macrophage polarization. Thus, LCN2 may represent a critical upstream regulator of inflammatory amplification in hypothermia-induced lung injury.

Several limitations should be acknowledged. First, LCN2 knockout animals were not used to validate the findings. Although AAV-mediated knockdown provided sufficient evidence to support the hypothesis, gene knockout models and transgenic rescue experiments would further confirm phenotypic specificity. Second, macrophage polarization was defined based on iNOS and Arg-1 expression alone. Given the growing complexity of macrophage subpopulations revealed by single-cell analyses[39-41], inclusion of additional markers would strengthen classification accuracy. Third, the downstream mechanisms by which LCN2 regulates macrophage polarization were not explored. LCN2 has been linked to iron metabolism, lipid metabolism, and ferroptosis[32,42]. Whether LCN2 modulates macrophage polarization in SH-ALI through metabolic reprogramming or ferroptosis-related pathways warrants further investigation.

In summary, this study establishes a reproducible rat model of SH-ALI and identifies LCN2 as a critical regulator of macrophage polarization and lung injury severity. Targeting LCN2-mediated inflammatory reprogramming of AMs may provide a novel therapeutic approach for severe hypothermia-induced lung injury.

5 Conclusion

In conclusion, the present study demonstrates that immersion in 15 °C seawater for 5 h reliably establishes a rat model of SH-ALI. This model is characterized by pronounced pulmonary inflammation, edema, and tissue damage, accompanied by a marked imbalance in macrophage polarization (Fig. 6). Excessive M1 polarization was observed in SH-ALI, indicating that pro-inflammatory macrophage activation plays a central role in disease progression. Importantly, LCN2 was significantly upregulated in SH-ALI, and its knockdown effectively attenuated lung injury, reduced inflammatory cytokine production, and improved survival. These protective effects were associated with suppression of M1 polarization, suggesting that LCN2 contributes to SH-ALI pathogenesis by promoting pro-inflammatory macrophage activation.

Future studies should further elucidate the molecular mechanisms by which LCN2 regulates macrophage polarization, including potential involvement of metabolic reprogramming, iron homeostasis, and ferroptosis-related pathways. A deeper understanding of these mechanisms may facilitate the development of targeted therapeutic strategies for SH-ALI.

Acknowledgments

The authors thank the International Science Editing (http://www.internationalscienceediting.com) for language editing services for this manuscript.

Research ethics

All animal experiments were conducted in accordance with the Guide for the Care and Use of Laboratory Animals, published by the US National Institutes of Health (NIH Publication No. 85-23, revised 1996). The study protocol was approved by the Animal Ethics Committee of the Chinese PLA General Hospital (approval number: SQ2022494).

Informed consent

Not applicable.

Author contributions

Chen X X and Han Z H conceived and design the present study. Zheng X and Ding Y W performed the experiments. Wang F and Zheng X. collected and analyzed the data. Wang F and Ding Y W interpreted the data and drafted the manuscript. All authors reviewed and approved the final version of the manuscript for publication.

Use of large language models, AI and machine learning tools

Not applicable.

Conflict of interest

The authors declare that they have no conflict of interest related to this study.

Research funding

The work was supported by the Innovative Cultivation Foundation of The Sixth Medical Center of PLA General Hospital [grant number CXPY202506].

Data availability

The datasets generated and analyzed during the current study are available from the corresponding author upon reasonable request.

References

[1] Tomassini L, Lancia M, Gambelunghe C, *et al.* Immunohistochemical insights into hypothermia-related deaths: A systematic review. Forensic Sci Med Pathol, 2025; 21: 1358-1369.

[2] Paal P, Pasquier M, Darocha T, *et al.* Accidental Hypothermia: 2021 Update. Int J Environ Res Public Health, 2022; 19(1): 501.

[3] Shahrbabak S M, Bouzid Z, Inan O T, *et al.* Physiology and enabling technologies for quantitative assessment of survivability during cold water immersion and rewarming: A review. Prog Biomed Eng (Bristol), 2025; 7(4): 1-23.

[4] Hleșcu A A, Grigoraș A, Ianole V, *et al.* Advanced diagnostic tools in hypothermia-related fatalities-a pathological perspective. Diagnostics (Basel), 2024; 14(7): 739.

[5] Ding Y, Xu Y, Wang J, *et al.* Cold-inducible RNA-binding protein causes prolonged immersion-induced hypothermic acute lung injury in a rat model through TREM-1 and NF-κB. Faseb J, 2025; 39: e70955.

[6] Liu J, Wu J, Qiao C, *et al.* Impact of chronic cold exposure on lung inflammation, pyroptosis and oxidative stress in mice. Int Immunopharmacol, 2023; 115: 109590.

[7] Shapiro K A, Phillips T C, Dineen E H, *et al.* The heart underwater: mechanisms and treatments of immersion pulmonary edema. Current Treatment Options in Cardiovascular Medicine, 2025; 19(27): 1075-1079.

[8] Wang Z, Wang Z. The role of macrophages polarization in sepsis-induced acute lung injury. Front Immunol, 2023; 14: 1209438.

[9] Liu C, Xiao K, Xie L. Advances in the regulation of macrophage polarization by mesenchymal stem cells and implications for ALI/ARDS treatment. Front Immunol, 2022; 13: 928134.

[10] Zhu G, Yu H, Peng T, *et al.* Glycolytic enzyme PGK1 promotes M1 macrophage polarization and induces pyroptosis of acute lung injury *via* regulation of NLRP3. Respir Res, 2024; 25: 291.

[11] Yan M, Tang J, Liu Y, *et al.* Progress of alveolar macrophages in biological function and acute lung injury/acute respiratory distress syndrome. Front Immunol, 2025; 16: 1683411.

[12] Deshpande D, Chhugani K, Chang Y, *et al.* RNA-seq data science: From raw data to effective interpretation. Front Genet, 2023; 14: 997383.

[13] Pasmanik-Chor M. Biological perspectives of RNA-sequencing experimental design. Methods Mol Biol, 2021; 2243: 327-337.

[14] Cheng L, Xing H, Mao X, *et al.* Lipocalin-2 promotes m1 macrophages polarization in a mouse cardiac ischaemia-reperfusion injury model. Scand J Immunol, 2015; 81: 31-38.

[15] Reynolds P, Wall P, Van Griensven M, *et al.* Shock supports the use of animal research reporting guidelines. Shock, 2012; 38: 1-3.

[16] Huang H, Wang J, Hussain S A, *et al.* Gossypin exert lipopolysaccharide induced lung inflammation *via* alteration of Nrf2/HO-1 and NF-κB signaling pathway. Environ Toxicol, 2023; 38: 1786-1799.

[17] Konkimalla A, Elmore Z, Konishi S, *et al.* Efficient Adeno-associated virus-mediated transgenesis in alveolar stem cells and associated niches. Am J Respir Cell Mol Biol, 2023; 69: 255-265.

[18] El Fakihi S, El Allam A, Tahoune H, *et al.* Functional characterization of small and large alveolar macrophages in sarcoidosis and idiopathic pulmonary fibrosis compared with non-fibrosis interstitial lung diseases. Hum Antibodies, 2023; 31: 59-69.

[19] Smith K M, Mrozek J D, Simonton S C, *et al.* Prolonged partial liquid ventilation using conventional and high-frequency ventilatory techniques: gas exchange and lung pathology in an animal model of respiratory distress syndrome. Crit Care Med, 1997; 25: 1888-1897.

[20] Tang J, Ding Y, Chen W, *et al.* VASP knockdown ameliorates lipopolysaccharide-induced acute lung injury with inhibition of M1 macrophage polarization through the cGMP-PKG signaling pathway. Inflammation, 2025; 48(5): 3458-3471.

[21] Wiberg S, Mortensen A F, Kjaergaard J, *et al.* Accidental hypothermia in Denmark: A nationwide cohort study of incidence and outcomes. BMJ Open, 2021; 11: e046806.

[22] Dickinson G M, Maya G X, Lo Y, *et al.* Hypothermia-related deaths: a 10-year retrospective study of two major metropolitan cities in the United States. J Forensic Sci, 2020; 65: 2013-2018.

[23] Bjertnæs L J, Næsheim T O, Reierth E, *et al.* Physiological changes in subjects exposed to accidental hypothermia: An update. Front Med (Lausanne), 2022; 9: 824395.

[24] Kulkarni H S, Lee J S, Bastarache J A, *et al.* Update on the features and measurements of experimental acute lung injury in animals: an official American thoracic society workshop report. Am J Respir Cell Mol Biol, 2022; 66: e1-e14.

[25] Chen X, Tang J, Shuai W, *et al.* Macrophage polarization and its role in the pathogenesis of acute lung injury/acute respiratory distress syndrome. Inflamm Res, 2020; 69: 883-895.

[26] Shan Q, Dong Z, Li N, *et al.* Deciphering the heterogeneity of pulmonary macrophages in response to fine particles. Small, 2026; 22: e07293.

[27] Speth J M, Bourdonnay E, Penke L R, *et al.* Alveolar epithelial cell-derived prostaglandin E2 serves as a request signal for macrophage secretion of suppressor of cytokine signaling 3 during innate inflammation. J Immunol, 2016; 196: 5112-5120.

[28] Morrison T J, Jackson M V, Cunningham E K, *et al.* Mesenchymal stromal cells modulate macrophages in clinically relevant lung injury models by extracellular vesicle mitochondrial transfer. Am J Respir Crit Care Med, 2017; 196: 1275-1286.

[29] Guardado S, Ojeda-Juárez D, Kaul M, *et al.* Comprehensive review of lipocalin 2-mediated effects in lung inflammation. Am J Physiol Lung Cell Mol Physiol, 2021; 321: L726-L733.

[30] Sciarretta F, Ceci V, Tiberi M, *et al.* Lipocalin-2 promotes adipose-macrophage interactions to shape peripheral and central inflammatory responses in experimental autoimmune encephalomyelitis. Mol Metab, 2023; 76: 101783.

[31] An H S, Lee J, Lee S J, *et al.* Lipocalin-2 deletion attenuates lipopolysaccharide-induced acute lung inflammation *via* downregulating chemotaxis-related genes. Biochem Biophys Res Commun, 2023; 652: 14-21.

[32] An H S, Yoo J W, Jeong J H, *et al.* Lipocalin-2 promotes acute lung inflammation and oxidative stress by enhancing macrophage iron accumulation. Int J Biol Sci, 2023; 19: 1163-1177.

[33] Wang X, Zhang C, Zou N, *et al.* Lipocalin-2 silencing suppresses inflammation and oxidative stress of acute respiratory distress syndrome by ferroptosis *via* inhibition of MAPK/ERK pathway in neonatal mice. Bioengineered, 2022; 13: 508-520.

[34] Lu F, Inoue K, Kato J, *et al.* Functions and regulation of lipocalin-2 in gut-origin sepsis: A narrative review. Crit Care, 2019; 23: 269.

[35] Du H, Liang L, Li J, *et al.* Lipocalin-2 alleviates LPS-induced

inflammation through alteration of macrophage properties. J Inflamm Res, 2021; 14: 4189-4203.
[36] Lindstrom E, Deis J, Bernlohr D A, *et al.* Lipocalin 2 in obesity and diabetes: insights into its role in energy metabolism. Endocrines, 2025; 6(1): 4.
[37] Jensen B L. Beyond being a biomarker: lipocalin-2/NGAL as a facilitator for protective drug action in hypoxic kidney injury. Acta Physiol (Oxf), 2025; 241: e70110.
[38] Zhang Z X, Peng J, Ding W W. Lipocalin-2 and intestinal diseases. World J Gastroenterol, 2024; 30: 4864-4879.
[39] Mitsui Y, Satoh T. Functional diversity of disorder-specific macrophages involved in various diseases. Inflamm Regen, 2025; 45: 29.
[40] Hume P S, Lyn-Kew K H, Wynn E A, *et al.* Spatial heterogeneity of macrophages in the human lung. (2025-05-30) [2026-03-02]. https://doi.org/10.1101/2025.05.30.657106.
[41] Chen X, Wang F, Tang J, *et al*. Paralemmin-3 augments lipopolysaccharide-induced acute lung injury with M1 macrophage polarization *via* the notch signaling pathway. Respir Physiol Neurobiol, 2024; 320: 104203.
[42] Lv Y, Zhang L. IRF7 Activates LCN2 Transcription to enhance LPS-induced acute lung injury by inducing macrophage ferroptosis and M1 polarization. Cell Biochem Biophys, 2025; 83: 2415-2430.